Phys. Plasmas **2** (8), August 1995, 3017

Wavelet bicoherence: A new turbulence analysis tool

B.Ph. van Milligen, E. Sánchez, T. Estrada, C. Hidalgo, B. Brañas
Asociación EURATOM-CIEMAT, Madrid, Spain
B. Carreras
Oak Ridge National Laboratory, Oak Ridge, Tennessee, U.S.A.
L.García
Universidad Carlos III, Madrid, Spain

Abstract

A recently introduced tool for the analysis of turbulence, wavelet bicoherence [B. Ph. van Milligen, C. Hidalgo and E. Sánchez, Phys. Rev. Lett. **16** (1995) 395], is investigated. It is capable of detecting phase coupling - nonlinear interactions of the lowest (quadratic) order - with time resolution. To demonstrate its potential, it is applied to numerical models of chaos and turbulence and to real measurements. It detected the coupling interaction between two coupled van der Pol oscillators. When applied to a model of drift wave turbulence relevant to plasma physics, it detected a highly localized coherent structure. Analyzing reflectometry measurements made in fusion plasmas, it detected temporal intermittency and a strong increase in nonlinear phase coupling coinciding with the L/H (Low - to - High confinement mode) transition.

PACS numbers: 02.70.Hm, 52.35.Mw, 52.35.Ra, 52.55.Hc

I Introduction: the analysis of turbulent data

The purpose of this paper is to elaborate on the interpretation and usefulness of a new analysis tool for chaos and turbulence that was recently introduced [1]. First, we will briefly comment on why we think a new tool is needed.

In the first place, although there has been considerable progress in the field of the analysis of chaotic or turbulent data in the ultimate years [2], yet the kind of analysis involving the determination of fractal dimensions, attractors, etc. is not always easily applicable to real data, especially when the noise contribution is significant. Furthermore, sometimes the information that can be recovered by these methods is not the most relevant to physical understanding: for example, while a measured low fractal dimension can be a very helpful information in working towards a physics model, a high dimension (significantly higher than 5, which is observed often in fusion plasmas [3]) leaves many questions open.

Secondly, the traditional analysis techniques involving long-time averages of moments of data and standard spectral methods are of limited applicability to chaotic or turbulent data. To see why this is so, consider the transition from (quasi-) periodicity to chaos in mathematical model systems. Generally speaking, three possible routes to chaos have been identified: period doubling, crises and intermittency [4]. Although sometimes modes are destabilized prior to the transition to chaos, all these routes have in common that the transition to chaos is abrupt and never a smooth continuation of the (quasi-) periodic state prior to the transition. A description of the chaotic state as a superposition of a large number of (harmonic) modes is therefore insatisfactory. In fact, it is known for some model systems that the equations describing these systems do not have a complete set of solutions, and therefore the observed behaviour cannot be decomposed into eigenmodes of the system. Thus it may be expected that a decomposition of observed states into Fourier harmonics (or other global modes), while suitable for global characterizations of chaos or turbulence by means of e.g. the decay of the spectrum with frequency, yields a confused picture on a finer scale, since it is not an optimal base for the expansion.

Thirdly, there are important indications from both numerical simulations and observation of twodimensional (2-D) and threedimensional (3-D) turbulence that turbulence generally is an intermittent phenomenon, i.e. localized in time and/or space [5]. Thus analysis techniques that presuppose homogeneity such as the Fourier decomposition do not seem very appropriate. The observed non-homogeneity of the turbulence is closely related with the concept of 'coherent structures'. These 'coherent structures' and their interactions would then hypothetically dominate the turbulent flow. This picture, although not sharply defined, provides the intuitive motivation for turning to wavelet analysis.

Wavelet analysis can be seen as a generalization of the Fourier analysis and in many cases permits a similar interpretation, but amplifies it by adding time resolution - in a more

fundamental way than is permitted by the Short-Time Fourier Transform, STFT, since the latter does not remove the objection raised above against Fourier-type methods.

Wavelet analysis has been applied with considerable success to turbulent data [5, 6, 7], but ways are needed to conveniently summarize and visualize the large amount of data generated by the wavelet transform, and extract the information relevant to non-linear interactions. For Fourier analysis the calculation of higher-order spectra has been applied with some success [8, 9, 10, 11]. In this paper the concept of the first higher-order spectrum (the bispectrum) is generalized to wavelet analysis.

The bicoherence, the normalized bispectrum, is a measure of the amount of phase coupling that occurs in a signal or between two signals. Phase coupling is defined to occur when two frequencies, ω_1 and ω_2, are simultaneously present in the signal(s) along with their sum (or difference) frequencies, and the sum of the phases ϕ of these frequency components remains constant. The bicoherence measures this quantity and is a function of two frequencies ω_1 and ω_2 which is close to 1 when the signal contains *three* frequencies ω_1, ω_2 and ω that satisfy the relation $\omega_1 + \omega_2 = \omega$ and $\phi_1 + \phi_2 = \phi + const$; if no such relation is satisfied, it is close to 0. When the analyzed signal exhibits *structure* of any kind whatever, it might be expected that some phase coupling occurs. Thus, the generalization of the bispectrum to wavelet analysis may be expected to be able to detect temporal variations in phase coupling (intermittent behaviour) or short-lived structures.

In Section II, a short formal description of wavelet analysis and wavelet bicoherence is given. Some remarks are made about the interpretation of the wavelet bicoherence in terms of features of the turbulence. The statistical error and noise level of the calculated bicoherence are estimated.

In Section III, the technique is applied to the output of some chaos and turbulence models and to measurement data. Two numerical models are analyzed: firstly, a system of two coupled van der Pol oscillators in both a periodic and a chaotic state; and secondly, a numerical model of drift wave turbulence in thermonuclear plasmas. The measurement data that are analyzed are taken with reflectometers in fusion plasmas.

Finally, in Section IV, some conclusions are drawn and possible applications of the technique are discussed.

II Wavelet analysis and wavelet bicoherence

II.a Introduction

Wavelet analysis has developed in the latter few years from a somewhat curious technique to a viable alternative to Fourier analysis; the mathematical foundations of the former are now as sound as those of the latter [12, 13].

Its invention was spurred by the need to analyze signals that contained rapidly changing frequencies, pulses or short temporal events (as may occur in turbulent data). These features cannot be resolved by Fourier analysis due to the fact that it involves an integral over time, such that the frequencies, pulses or events are averaged out - if the averaging does not obliterate the frequency 'finger print' of the events, then at least it eliminates the temporal information, such that from the Fourier analysis it is not possible to reconstruct *when* the pulse or event has taken place (the Short-Time Fourier Transform, STFT, to some extent resolves this problem although perhaps not in an optimal way, depending on the requirements; in any case the fundamental objection to a decomposition in harmonics mentioned in Section I is not tackled with the STFT).

Wavelet analysis takes as its analyzing basis functions wavelets, i.e. (oscillating) functions that decay rapidly with time, rather than sines and cosines that have no such decay. Thus, a wavelet transform at a given time point is similar to a Fourier transform in the sense that it exhibits the contribution of the different frequencies to the signal, but due to the decay of the wavelet this information only pertains to a certain short time interval of the signal. When the wavelet transform is carried out on successive time intervals, the contributions of the various frequencies to the signal can be followed in time. In effect, a wavelet transform is therefore not only a function of frequency, but also of time.

Rather than referring to frequency, the wavelet transform is usually expressed in terms of the *scale* of the analyzing wavelet, which can be understood to be proportional to the inverse frequency. The kind of wavelet analysis described above and used in the remainder of this paper is the *continuous wavelet transform*, but we wish to mention that the corresponding *discrete* or *fast wavelet transform* also exists; it is based on orthogonal wavelets, guaranteeing that the wavelet transform contains exactly the same information as the original signal and can be unequivocally reconstructed from its transform (just as with the Fast Fourier Transform, FFT) [12, 14]. The reason we prefer to use the continuous wavelet transform in the present work will become clear below.

II.b Formal description

The Fourier transform of a function *f(t)* and its power spectrum are given by:

$$\hat{f}(\omega) = \int_{-\infty}^{\infty} f(t) e^{-i\omega t}\, dt \qquad \text{and} \qquad P_f(\omega) = \left|\hat{f}(\omega)\right|^2 \tag{1}$$

A wavelet can be any function $\Psi(t)$ that satisfies the *wavelet admissibility condition:*

$$c_\Psi = \int_{-\infty}^{\infty} \left|\hat{\Psi}(\omega)\right|^2 |\omega|^{-1}\, d\omega < \infty \tag{2}$$

The corresponding wavelet family is obtained by means of the scale length parameter *a*:

$$\Psi_a(t) = \frac{1}{a^p}\Psi(t/a) \tag{3}$$

Some authors prefer to use the scale number *s* instead, where *s = 1/a*. The scale number *s* is proportional to the frequency of the wavelet. The factor *p* is the normalization choice. In literature, values of *p* of 0, 1/2 and 1 are encountered [7, 14]. In the present work, we choose *p* = 1/2; with this choice, the L^2-norm of the wavelet is independent of *a*. Other choices, although perhaps helpful for purposes of visualization of the wavelet power spectrum, would hamper the interpretation of the wavelet bicoherence (see below).

The wavelet transform of a function *f(t)* is then given by:

$$W_f(a,\tau) = \int f(t)\Psi_a(t-\tau)\,dt \tag{4}$$

$W_f(a,\tau)$ at any given *a* can be interpreted as a filtered version of *f(t)*, bandpassed by the filter Ψ_a. Usually $|W_f(a,\tau)|^2$ is plotted in the (a,τ) - plane for visualization purposes (scalogram). Observe that for the continuous wavelet transform, Eq. (4), the wavelets are not orthogonal and the transform contains redundant information. Nevertheless, the corresponding inverse wavelet transform (for *p* = 1/2) can be calculated (for almost all *t*) by:

$$f(t) = \frac{1}{c_\Psi}\iint W_f(a,\tau)\Psi_a^*(\tau-t)\frac{da\,d\tau}{a^2} \tag{5}$$

In some sense, the wavelet transform can be regarded as a generalization of the Fourier transform. The main advantage over the Fourier transform is that, with a suitable choice of wavelet Ψ, time-resolved spectra can be calculated. Here we give the definition of various combined spectra. In order to obtain statistical stability (discussed in section II.d) while maintaining time resolution, these are evaluated by integrating over a finite time interval *T*: $\tau_0 \le \tau \le \tau_1$. Apart from that, the definitions are completely analogous to the usual definitions used in Fourier analysis.

The wavelet cross spectrum is given by:

$$C_{fg}^w(a) = \int_T W_f^*(a,\tau)W_g(a,\tau)\,d\tau \tag{6}$$

where *f(t)* and *g(t)* are two time series. We also introduce the *delayed* wavelet cross spectrum:

$$C_{fg}^w(a,\Delta\tau) = \int_T W_f^*(a,\tau)W_g(a,\tau+\Delta\tau)\,d\tau \tag{6b}$$

which is a useful quantity for detecting e.g. structures flowing past two separated observation points. The normalized delayed wavelet cross coherence is:

$$\gamma_{fg}^w(a,\Delta\tau) = \frac{\left|\int_T W_f^*(a,\tau)W_g(a,\tau+\Delta\tau)\,d\tau\right|}{\left(P_f^w(a)P_g^w(a)\right)^{1/2}} \tag{6c}$$

which can take on values between 0 and 1. Here the wavelet auto-power spectrum is given by:

$$P_f^w(a) = C_{ff}^w(a) \tag{7}$$

Note that the wavelet power spectrum can also be written in terms of the Fourier power spectra of the wavelet and *f(t)*:

$$P_f^w(a) = \frac{1}{2\pi}\int P_{\Psi_a}(\omega) P_f(\omega)\, d\omega, \tag{8}$$

where $P_f(\omega)$ is evaluated on *T*. Thus, the wavelet power spectrum is the Fourier power spectrum averaged by the power spectrum of the wavelet filter [6].

We introduce the first higher-order spectrum along the same lines. By analogy to the definition of the bispectrum in Fourier terms as in Ref. 10, we define the wavelet cross-bispectrum as in Ref. 1:

$$B_{fg}^w(a_1, a_2) = \int_T W_f^*(a,\tau) W_g(a_1,\tau) W_g(a_2,\tau)\, d\tau \tag{9}$$

where

$$\frac{1}{a} = \frac{1}{a_1} + \frac{1}{a_2} \qquad \text{(frequency sum-rule)} \tag{10}$$

The wavelet cross-bispectrum measures the amount of phase coupling in the interval *T* that occurs between wavelet components of scale lengths a_1 and a_2 of *g(t)* and wavelet component *a* of *f(t)* such that the sum rule is satisfied. If the scale lengths may be interpreted as inverse frequencies, $\omega = 2\pi/a$ (whether this is permitted depends on the wavelet type - it is valid for wavelets whose Fourier spectrum has a single well-defined peak), one may interpret the wavelet cross-bispectrum as the coupling between waves (wavelets) of frequencies such that $\omega = \omega_1 + \omega_2$. Likewise, we define the wavelet auto-bispectrum

$$B^w(a_1, a_2) = B_{ff}^w(a_1, a_2) \tag{11}$$

The squared wavelet cross bicoherence is the normalized squared cross-bispectrum:

$$\left(b_{fg}^w(a_1, a_2)\right)^2 = \frac{\left|B_{fg}^w(a_1, a_2)\right|^2}{\left(\int_T \left|W_g(a_1,\tau) W_g(a_2,\tau)\right|^2 d\tau\right) P_f^w(a)} \tag{12}$$

which can attain values between 0 and 1. Similarly, the squared wavelet auto-bicoherence (henceforth simply referred to as bicoherence) is

$$\left(b^w(a_1, a_2)\right)^2 = \left(b_{ff}^w(a_1, a_2)\right)^2 \tag{13}$$

It is convenient to introduce the summed bicoherence, which is defined as $\backslash B(b^w(a))^2 = \frac{1}{s(a)} \sum \left(b^w(a_1,a_2)\right)^2$ where the sum is taken over all a_1 and a_2 such that Eq. (10) is satisfied and *s(a)* is the number of summands in the summation. Similarly, the total bicoherence is defined as $\left(b^w\right)^2 = \frac{1}{S} \sum\sum \left(b^w(a_1,a_2)\right)^2$ where the sum is taken over all a_1 and a_2 and *S* is again the number of terms in the summation. The factors *s(a)* and *S*, additions to the earlier definitions

given in Refs. 15 and 1, guarantee that the summed and total bicoherence are bounded between 0 and 1. These quantities summarize the information conveniently, as will be seen later.

Up to this point, the exact form of the wavelet did not enter the definitions. But in order to discuss the interpretation of the bicoherence, we need to choose a wavelet type suited for this kind of analysis. As was suggested above, the coupling between wavelets only makes sense when a frequency can be assigned to the wavelet. Thus, we restrict our attention to wavelets which have Fourier transforms that exhibit a single dominant peak, and define the location of that peak as the corresponding frequency.

In literature, several suitable wavelets are mentioned. Cubic spline wavelets [13], for example, would provide an excellent basis for the analysis. In the present work, however, we have chosen the following conceptually simple wavelet in order to ease the interpretation of the results:

$$\Psi_a(t) = \frac{1}{\sqrt{a}} \exp\left[i\frac{2\pi t}{a} - \tfrac{1}{2}\left(\frac{t}{ad}\right)^2 \right] \qquad (14)$$

The parameter d determines the exponential decay of the wavelet and thus permits a suitable combination of time- and frequency resolution to be selected. The real and imaginary parts of this wavelet are shown in Fig. 1 for $d=1$, along with its Fourier transform. The simplicity in the interpretation results from the fact that to each a corresponds a frequency $\omega = 2\pi/a$. The frequency resolution of the wavelet is approximately $\Delta\omega = \omega/4d$ (FWHM - Full Width at Half Maximum). The time resolution is $\Delta t = ad$, given by the decay of the exponential part of the wavelet. As d increases, frequency resolution improves but time resolution deteriorates. For $d >> 1$ the wavelet analysis effectively becomes a Fourier analysis. We set $d=1$ in the following, which is, we believe, a reasonable compromise between frequency and time resolution, although for specific purposes other choices may be better. Note that we do not impose the condition that the wavelets be orthogonal, because we wish to choose the frequencies in the analysis procedure freely, and not be restricted to $a \in \{2^n\}$ [6, 12, 14]. This implies a certain redundancy in the wavelet transform coefficients which must be taken into account upon interpreting the results (cf. section II.d).

The squared bicoherence $\left(b^w(a_1,a_2)\right)^2$ is usually plotted in the (ω_1,ω_2) - plane rather than the (a_1,a_2) - plane for ease of interpretation. We allow ω_1, ω_2 and ω to take on negative values in order to be able to represent all sum and difference combinations of ω_1 and ω_2 . There is no need to represent the whole plane; firstly, both ω_1, ω_2 and their sum ω must be smaller than the Nyquist frequency (half the sampling frequency); secondly, because ω_1 and ω_2 are interchangeable, we may restrict the plot to $\omega_1 \geq \omega_2$; and finally, the case (ω_1,ω_2) is identical to the case $(-\omega_1,-\omega_2)$ which is therefore not represented.

II.c Interpretation of the wavelet bicoherence

The significance of the squared wavelet bicoherence can perhaps best be understood by analyzing a few examples and contrasting the results with the results that would be obtained with the Fourier-based bicoherence analysis. If one generates a test signal *f(t)* given by:

$$f(t) = A_p \sin(\omega_p t) + A_q \sin(\omega_q t) + A_r \sin(\omega_r t) \qquad (15)$$

such that the coupling condition $\omega_p = \omega_q + \omega_r$ is satisfied and A_p, A_q and A_r are constants, three peaks with amplitude 1 will appear in the (ω_1,ω_2) - plane: one at $\omega_1 = \omega_q$, $\omega_2 = \omega_r$, one at $\omega_1 = \omega_p$, $\omega_2 = -\omega_r$ and one at $\omega_1 = \omega_p$, $\omega_2 = -\omega_q$. This is basically the same result as obtained with the bicoherence based on Fourier analysis [8, 9]. However, the coupling condition $\omega_p = \omega_q + \omega_r$ need only be satisfied to within the frequency resolution (discussed above) to produce a high value of the bicoherence, which in some cases is a significantly less strict requirement than with the Fourier-based analysis. For example, if there is a mismatch in coupling frequencies $\Delta\omega$ such that $\omega_p = \omega_q + \omega_r + \Delta\omega$, and $\Delta\omega$ is larger than the frequency resolution of the Fourier analysis but smaller than the wavelet frequency resolution corresponding to the highest frequency of the set $\{\omega_p, \omega_q, \omega_r\}$, then the wavelet bicoherence will show high bicoherence where the Fourier bicoherence detects low bicoherence. Decreasing the exponential decay (by increasing *d*) of the wavelet, Eq. (14), improves the frequency resolution such that the wavelet results gradually approximate the Fourier results.

A similar test signal that is mostly random noise, except for a short period in which phase coupling is generated in the manner of Eq. (15), may cause the Fourier-based bicoherence not to detect the coupling due to the large time window used in its averaging process, whereas the wavelet bicoherence will detect the coupling during the relevant time window (provided it has a certain minimum duration, discussed in Section II.d). This feature allows *intermittent coupling* to be detected; further, the time when the coupling occurs can be identified along with the *scales of the coupling interaction*. An interesting practical application of the wavelet bicoherence is therefore its use as a detector of intermittent non-linear behaviour (cf. section III.c).

It will be noted that in the three subregions of the region we have selected for representation of the bicoherence $\{\omega_2 > 0\}$, $\{\omega_2 < 0 \wedge \omega_1 > -2\omega_2\}$ and $\{\omega_2 < 0 \wedge \omega_1 < -2\omega_2\}$, the bicoherence differs only in normalization (cf. Eqs. (9) and (12)), the squared bispectrum being the same; therefore, in many cases a triple symmetry will appear in the plot. The symmetry can be broken, for example, by letting the amplitudes A_p, A_q and A_r of the test signal (Eq. (15)) vary slowly in time: then the heights of the three peaks will differ. This occurs often when analyzing measurement data, and is an indication that the coupling strength varies during the time window of analysis.

At this point, a caveat is in place: when the test signal is periodic but non-sinusoidal (e.g. a square wave or a sawtooth), very strong coupling will be detected for a wide range of

frequencies. This is as expected, since the non-sinusoidal wave can be built up from a number of Fourier components that are phase-locked with respect to each other. In fact, this reveals a fundamental difficulty when analyzing data taken e.g. at one point in a turbulent fluid: it is not possible to discern between the coupling generated by a static structure (eddie) passing by the observation point and a dynamic wave-interaction process. To some extent, this problem can be alleviated by analyzing data from various observation points (see below).

The interpretation of the bicoherence in terms of the underlying physics is, in general, not straight-forward. The simplest interpretation is offered by a quadratic coupling model [9, 10, 16], which is relevant to the description of some drift-wave turbulence in plasmas. In this model, the coupling between three 'modes' or 'scales' a, a_1 and a_2 is expressed by means of a *coupling constant* $A(a_1, a_2, \tau)$:

$$W_f(a,\tau) = W_f^0(a,\tau) + A(a_1,a_2,\tau)W_g(a_1,\tau)W_g(a_2,\tau),$$

where the frequency sum-rule (Eq. 10) is satisfied. The component $W_f^0(a,\tau)$ is statistically independent of any other scales a_i. This equation expresses the existence of a (quadratic) relation between the three wavelet components. When the coupling constant $A(a_1, a_2, \tau)$ changes little during the time T used in the averaging process (cf. Eq. 9), the following equivalence holds:

$$\left|A(a_1,a_2,\tau')\right|^2 \approx \frac{\left|b_{fg}^w(a_1,a_2)\right|^2 P_f^w(a)}{\int_T \left|W_g(a_1,\tau)W_g(a_2,\tau)\right|^2 d\tau}$$

where τ' is the central value of the averaging time interval T. Thus, the coupling constant in this simple quadratic phase-coupling model can be determined by evaluating the bicoherence, provided the averaging time T is smaller than the rate of change of the coupling constant.

More detailed interpretations are possible when data from more than one observation point are available. For example, two closely spaced observation points in a turbulent field allow the calculation of the cross-bicoherence. This analysis has two advantages over the single-point measurement: firstly, any random noise present in the measurements will be more effectively suppressed provided the two measurements may be considered statistically independent; and secondly, the cross-bicoherence decreases when the two points are separated, such that a determination of the average or typical size of each of the structures is possible (of course, the fluid velocity along the line connecting the two measurement points has to be taken into account - in some cases the cross correlation can give an estimate of this quantity). Finally, with an array of measurement points both time- and space-resolved (wavelet) spectra and (bi-) coherencies can be evaluated.

II.d Error estimation

In the following, we discuss the statistical noise contribution to and the error estimate of the wavelet bicoherence. The noise contribution results from the fact that one is integrating over finite times in order to calculate the bicoherence. We call this the statistical noise level because it is the value of bicoherence that would be attained by a white noise input signal, and is caused by finite statistics (i.e. using a limited number of values in the integrating or averaging process). Likewise, the error estimate we give is the product of the uncertainties in the determination of the individual wavelet coefficients.

As was mentioned earlier, the wavelet bicoherence is calculated by integrating over a time interval *T*. Since the signals to be analyzed are usually digitally sampled, one may express *T* in terms of a number of samples, *N*. If we assume, for the moment, that all estimates of wavelet coefficients are independent, then the average bicoherence suffers a statistical error of $1/\sqrt{N}$ due to the summation over *N* values. A similar argument holds for the Fourier-based bicoherence, but here the summation is carried out over *N/M* ensembles, where *M* is the number of points in each statistically independent ensemble for which the *M*-points Fourier transform is calculated, where *M* typically is 128 points. Thus the statistical error in the Fourier-based bicoherence only decays as $\sqrt{M/N}$, and a factor of *M* more points are needed to obtain the same statistical errors as with the wavelet method. In this sense, the wavelet bicoherence represents a significant improvement in the time resolution of the bicoherence analysis (typically, by a factor of 128).

However, the wavelet coefficients are not all statistically independent, since the chosen wavelet family is not orthogonal. Each coefficient is calculated by evaluating Eq. (4), integrating over the range $-\infty < t < \infty$. Due to the periodicity *a* of the wavelets of scale *a* (cf. Fig. 1), two statistically independent estimates of the wavelet coefficients are separated by a time *a/2*, or by a number of points $M(a) = a\omega_{samp}/4\pi$ (ω_{samp} being the sampling frequency). Thus, the summation done in the evaluation of the bicoherence $b^w(\omega_1,\omega_2)$ is not really carried out over *N* points, but only over $N/\max(M(a))$, where the maximum is taken over the values of *a* that come into play for the evaluation of a specific value of the squared bicoherence. An estimate for the statistical noise level in $b^w(\omega_1,\omega_2)$ is, therefore:

$$\varepsilon\left(b^w(\omega_1,\omega_2)\right) \approx \left[\frac{\omega_{samp}/2}{\min(|\omega_1|,|\omega_2|,|\omega_1+\omega_2|)}\frac{1}{N}\right]^{1/2} \qquad (16)$$

Observe that at low frequencies the statistical noise may dominate the bicoherence, and a significant interpretation must limit itself to (relatively) high frequencies.

The statistical error in the determination of $b^w(\omega_1,\omega_2)$ can be deduced from Eq. (12). Each factor in this equation that is obtained by integrating over *T* suffers an error of $1/\sqrt{N}$, so that the error is estimated by:

$$\frac{\Delta\left(b^w(\omega_1,\omega_2)\right)}{b^w(\omega_1,\omega_2)} \approx \frac{2}{\sqrt{N}} \qquad (17)$$

Note that Eqs. (16) and (17) imply that the bicoherence analysis is able to detect coherent signals in extremely noisy data, provided the coherency remains constant during sufficiently long times, since the noise contribution falls off rapidly with increasing N: If one demands, for exampe, that the bicoherence due to the coherent signal should be at least a factor 3 above the maximum noise contribution, the allowable signal-to-noise ratio is 3ε (ε given by Eq. (16)), which in many cases (N sufficiently large) is well below 1. In this sense, the bicoherence can be considered a very powerful noise filter.

Fig. 2 presents an analysis of random data, sampled at 1 MHz, with a Gaussian probability distribution function (PDF). The summed bicoherence graphs are calculated for sections of data with N = 200, 400, 800 and 1600. It is observed that the calculated bicoherence falls with increasing N roughly as is predicted by Eq. (16) (dashed lines).

II.e Comparison wavelet and Fourier bicoherence

In order to compare the wavelet and Fourier-based bicoherence, measurements taken at the Advanced Toroidal facility (ATF) [17] with Langmuir Probes and with known strong Fourier bicoherence were analyzed (see Ref. 18 for a more detailed description of these data). The data record consists of 16384 data points sampled at 1 MHz. The first data point is taken to occur at 0 ms.

Figure 3a shows the wavelet and the smoothed Fourier spectrum (calculated for a data section running from 1 to 9.192 ms) showing the base-10 logarithm of the spectral power. The spectrum is clearly turbulent with no dominant modes.

Figure 3b shows both the Fourier and wavelet bicoherence graphs, calculated on a frequency grid with 64 grid points from 0 to 500 kHz from a data section running from 1 to 16 ms. Although the wavelet graph shows much less detail, as is expected from the lower frequency resolution (Section II.b), the overall features are similar, and the values of bicoherence agree quite well.

Figure 3c (top) shows the summed bicoherence for both the Fourier and Wavelet bicoherence. Due to better statistics, the noise level in the wavelet graph is much lower than in the Fourier graph (Section II.d). Nevertheless, the values of the bicoherence in the range $f <$ 150 kHz, where the Fourier bicoherence is still above noise level, agree quite well with the wavelet bicoherence. Of course, the wavelet graph shows less detail due to its lower frequency resolution.

To demonstrate that the bicoherence in both cases is detecting something that is not evident from the Fourier spectrum, we performed an FFT on the raw data, scrambled the phase information (i.e., maintaining the FFT transform coefficient amplitudes, we gave each coefficient a random phase), and performed an inverse FFT to obtain a new data series. It is expected that this new series exhibits no coherence of any kind, even though its power

spectrum is identical to the original series. Effectively, as is shown in Fig. 3.c (bottom), both the Fourier and wavelet bicoherence drop to noise level.

III Analysis of simulated and experimental data

III.a Simulated data: Coupled van der Pol oscillators

In the present section, data from a system of two coupled van der Pol oscillators are analyzed. This system of oscillators is one of the simplest that exhibits chaos in a self-sustaining way, i.e. without external driving [19]:

$$\frac{\partial x_i}{\partial t} = y_i$$
$$\frac{\partial y_i}{\partial t} = \left[\varepsilon_i - \left(x_i + \alpha_j x_j\right)^2\right] y_i - \left(x_i + \alpha_j x_j\right)$$

The system {i=1, j=2} describes the first oscillator, whereas {i=2, j=1} describes the second. The ε_i describe the limit cycles of the oscillators and the α_j the nonlinear coupling between them. Further detail is provided in Ref. 19.

The analysis of the behaviour of this system as a function of its control parameters has been done to some depth in the cited reference and will not be repeated here. We analyze the output data $x_2(t)$ of the system for two combinations of control parameters as given in Table 1.

The Fourier spectrum of the signal $x_2(t)$ in the periodic case is shown in Fig. 4a. The very clean spectrum shows only a few peaks with their harmonics. A section of 153 data points, sampled every $\Delta t = 0.2$ (units see Ref. 19) and covering about 5 periods of the x_2 coordinate, was analyzed using the wavelet bicoherence method. Because the signal does not contain high frequency components, the wavelet coefficients decay to very low values at those frequencies. To prevent computer rounding errors at those frequencies, a small random signal (with an amplitude of roughly 10^{-4} times the signal RMS - Root Mean Square - value) was added to the data. The result of the calculation is shown in Fig. 4b. The ridges near zero frequency are not significant since they are below the statistical noise level (Eq. (16)). The strong, straight horizontal and diagonal ridges correspond to a frequency of roughly 0.34, which can be identified in Fig. 4a with the second peak. Thus, the two dominant peaks in the Fourier spectrum at frequencies of 0.17 and 0.51 couple with their difference frequency at 0.34. Likewise, the difference in frequency between the second and the fourth peak, between the fourth and the sixth peak, etc., is allways 0.34, and the same holds for the odd series of peaks. The difference frequencies between even and odd peaks (i.e. 0.17) are not reflected in the bicoherence plot, however (except when coupled to 0.34). It may therefore be conjectured that the odd peaks are the harmonics of the limit cyle of the oscillators, whereas the even peaks

are due to the coupling interaction between the two oscilators. This interpretation is reaffirmed by the knowledge that with the combination of control parameters as given the limit cycle is asymmetric, which means that, were the coupling constants zero, only odd harmonics would appear [19].

The Fourier spectrum of the signal $x_2(t)$ in the chaotic case is shown in Fig. 4c. Several peaks are still visible, and some of these are related to the peaks in the periodic case through a frequency shift. New peaks have also appeared due to the process of period doubling in the transition to chaos. The chaos is apparent in the increase of the noisy (broad-band) part of the spectrum. Fig. 4d shows the bicoherence as calculated using a section of 303 data points, sampled every $\Delta t = 0.2$, that covers about 8 pseudo-periods of $x_2(t)$. At first view, there is a striking similarity to Fig. 4b. The main horizontal and diagonal ridges occur at a frequency of about 0.25, corresponding to the fourth major peak in Fig. 4c. This frequency must therefore be identified with the frequency of 0.34 in Fig. 4a - the change of control parameters of the coupled system, apart from introducing chaos, causes an overall frequency downshift with a factor of 0.73. Further it is observed that, although the high-frequency aspect of the graph has changed little - apart from a reduction in the value of the squared bicoherence -, the low-frequency part is much more complex. The vertical line indicating the simple coupling at 0.34 of Fig. 4b has split into several distinct coherent points at slightly shifted frequencies; observe the similarity in shape of these three points with the three points at double the frequency, which is obviously related to the period doubling process. New couplings have appeared at even lower frequencies (below 0.2), the biggest of which, at around 0.13, is easily identified as half the main coupling frequency of 0.25, and which is due to the period doubling effect also apparent in Fig. 4c.

III.b Simulated data: Plasma drift wave turbulence model

The numerical results analyzed in this section correspond to a simple model of long-wavelength drift wave turbulence [20]. We use a sheared-slab geometry. In this approximation, the equilibrium quantities vary along the *x*-axis (radial direction) but are independent of the other two coordinates, *y* (poloidal direction), and *z* (toroidal direction). The equilibrium magnetic field is

$$\vec{B} = B_0\left(\hat{z} + \frac{x}{L_s}\hat{y}\right),$$

where L_s is the magnetic shear length and $\hat{y}$ and $\hat{z}$ are the unit vectors in the *y* and *z* directions, respectively. In addition to the magnetic field, the equilibrium is characterized by the electron density and temperature profiles with basic scale lengths L_n and L_T, respectively.

The simplified drift wave model, valid for long wavelengths, is

$$\frac{d\tilde{n}_i}{dt} + V_{*n}\frac{d\tilde{n}_i}{dy} - L_n D_0\left[\vec{\nabla}_\perp\left(\frac{\partial\tilde{n}_i}{\partial y}\right)\times\hat{z}\right]\cdot\vec{\nabla}_\perp\tilde{n}_i + D_0\frac{\partial^2\tilde{n}_i}{\partial y^2} - \rho_s^2\frac{d\nabla_\perp^2\tilde{n}_i}{dt} - \frac{c_s^2}{\nu_i}\nabla_\parallel^2\tilde{n}_i = 0.$$

This is the model used in the numerical calculations.

The ion density is separated into averaged and fluctuating components. the fluctuating part of the density is indicated by a tilde and is written as a Fourier expansion:

$$\tilde{n}_i(x,\theta,\varsigma) = \sum_{\substack{m,n \\ n>0}}\left[\tilde{n}_{m,n}(x)\cos(m\theta + n\varsigma) + \tilde{n}_{-m,n}(x)\sin(m\theta + n\varsigma)\right]$$

here θ and ζ are the poloidal and toroidal angles, respectively. In slab geometry, they are related to the *y* and *z* coordinates by by $y = x_0\theta$ and $z = R_0\zeta$. The poloidal and toroidal mode numbers are defined as $m = x_0 k_y$ and $n = R_0 k_z$, respectively. In the numerical calculations, the coordinate *x* is not defined with relation to any singular surface; its value at the centre of the computational box is $x = x_0$. The boundary condition is that the density is zero at the conducting wall, $x = x_0 - a/2$ and $x = x_0 + a/2$. Here, *a* is the width of the computational box. To complete the numerical representation of the fields, we use finite differences in the radial coordinate *x*.

The equilibrium parameters for the nonlinear calculations are $L_s/L_n = 20$, $\rho_s/L_n = 3.6 \times 10^{-3}$, $L_T/L_n = 1$, $x_0 = 277\rho_s$, $D_0 = 0.025\rho_s c_s$, and $D_\parallel = 2.4 \times 10^5 \rho_s c_s$. The value of $D_\parallel$ has been chosen to provide a range of unstable modes with $6 \le m \le 76$. The safety factor *q* is equal to $\frac{3}{2}$ at the centre of the computational box. The standard box size is $60\rho_s$, and the number of unstable modes with resonant surfaces inside the computational box is about 250. In the calculation, we have included 439 Fourier components. The averaged density gradient is fixed, so saturation is caused by turbulence effects. The numerical data are for the saturated state.

Fig. 5a shows the RMS fluctuation level for this simulation, averaged over the time interval $30.2 \times 10^4 < \Omega_i t < 40.4 \times 10^4$ (the time step, in these units, is 100), versus radius (given in units of ρ_s). The RMS level peaks at the position of the position of the $q = \frac{3}{2}$ rational surface. Fig. 5b shows the wavelet spectrum of the same data, calculated over the interval $31.1 \times 10^4 < \Omega_i t < 39.4 \times 10^4$. Not the whole data time window is used because the continuous wavelet transform cannot be evaluated near the data edges. The frequency is given in inverse time units. The wavelet spectrum broadens where the RMS level is high. At radial positions where the spectrum is narrow, the calculation of the wavelet transform suffers from numerical errors at high frequency. This is important to keep in mind when viewing the results presented in Fig. 6.

Fig. 6a shows the total bicoherence vs. radial position for this simulation. Fig. 6b shows the corresponding summed bicoherence as a function of both sum frequency and radial position. From Fig. 6b it is apparent that e.g. the peak in Fig. 6a at 47.5 ρ_s is due mainly to the numerical problems mentioned above and does not correspond to anything physical. Thus one should ignore the bumpy structures at radial positions and frequencies where such numerical problems occur (roughly, to the right of the dashed line in Fig. 6b, which is the -10 level of

Fig. 5b). Examining the remainder of Figs. 6a and b, one can make the following observations: (1) The bicoherence drops sharply at the position of the $q = \frac{3}{2}$ rational surface, located at 30 ρ_s (whereas nor the RMS value, nor the spectrum exhibit such a local drop). (2) The maximum of the bicoherence is at 31 ρ_s. (3) Secondary maxima occur, apart from some minor peaks, at 16.5, 24.5, 29.5 and 36.5 ρ_s. These positions coincide roughly (but *not* exactly) with maxima in the RMS value (see Fig. 5a). From this, we conclude that the bicoherence provides information that pertains to an aspect of the turbulence (non-linear, or rather quadratic behaviour) that is not captured by either of the other methods.

Having established the general interest of this analysis, the next question must be: how does this information help in understanding turbulence? In the following, we compare the results from the bicoherence calculation with a more conventional approach. Fig. 6c shows the cross correlation, the weighted average cross coherence and the weighted average cross phase between one radial position and the next; the weighting being done by the spectral power (the cross spectra are calculated with the normal FFT). It is observed that the cross correlation and cross coherence between adjacent radial positions is generally high, but that around 30 ρ_s these quantities drop. Further, it is observed that the cross phase exhibits a peak around 30.5 ρ_s, possibly indicating shear flow. The numerical results also show the existence of a shear flow layer in this location. Although this analysis is by no means conclusive, it seems to suggest an explanation of the drop in bicoherence at 30 ρ_s in terms of a decorrelation of the turbulence, possibly linked to a shear flow.

The maximum in the bicoherence at 31 ρ_s is related to the presence of a long-living structure that is highly localized poloidally and radially. This structure has the (3,2) periodicity and lies close to the $q = \frac{3}{2}$ surface; such a structure is visible in a two-dimensional plot of the ion density, but because of its high spatial localization, it was only discovered after this analysis indicated the persistence of non-linear couplings over a time period of many decorrelation times (in Ref. 20 it is explicitly indicated that coherent structures were not seen).

For a more detailed analysis we refer to Fig. 6d, where the full bidimensional bicoherence is shown for a few selected radial positions. First, we draw attention to the graph corresponding to 30 ρ_s. Here the typical behaviour of a single mode coupling to broad-band turbulence is visible (horizontal band-like structure), with the main mode frequency around 1.4×10^{-4}. Turning now to the graph taken at the maximum of the bicoherence (at 31 ρ_s), one observes that each point of this band-like structure couples, in its turn, to a range of frequencies, thus nearly filling the two-dimensional plane of the bicoherence. A similar thing occurs at 29.5 ρ_s (here also a harmonic of the mode can be seen). Then, at 24.5 ρ_s, a completely different picture arises. An independent, but far weaker, mode is visible at a different frequency. A similar statement can be made about 16.5 ρ_s (recall that the structure at higher frequencies is numerical noise).

III.c Intermittency: Reflectometry data from ATF

We have analyzed data taken with a dual sin/cos reflectometer [21] in the edge region of the Advanced Toroidal Facility (ATF). This is an $l = 2$, $M = 12$ torsatron with major radius $R_0 = 2.10$ m and minor radius $a = 0.27$ m. The toroidal magnetic field is $B = 0.95$ T. The plasma has a line average electron density of $\bar{n}_e = 5 \times 10^{18}$ m^{-3}, a central electron temperature of $T_e = 850$ eV, and is heated with $P_{ECH} = 360$ kW of Electron Cyclotron Resonant Heating (ECRH) power. The stored energy is approximately 1.9 kJ. The data are taken during the flat-top (quasi-static equilibrium) phase of the discharge, and pertain to a normalized radial position of approximately r/a = 0.73 (channel 5) and 0.76 (channel 6). The data exhibit both very strong Fourier and wavelet bicoherence.

Fig. 7a shows the total bicoherence vs. time. The spiky behaviour is a clear indication of turbulent intermittency. Such behaviour has been reported before on the same device with data from Langmuir probes (cf. [1]). The summed bicoherence graphs at various selected times, also shown in Fig. 7a (for channel 5), show that the temporal increment of the coupling is mainly due to high frequencies (above 100 kHz); this again in accordance with the earlier observations with Langmuir probes [1]. Also shown is the corresponding wavelet spectrum. Fig. 7b shows a series of bicoherence plots corresponding to the selected time intervals of Fig. 7a (for channel 5). Note the horizontal and diagonal structures corresponding to the coupling of a mode to broad-band turbulence. Further, observe that the graphs corresponding to high bicoherence (11-12 ms and 14-15 ms) are similar to the graphs of the simulations done by Carreras of drift-wave turbulence with 439 modes at 31 ρ_s (Fig. 6d).

III.d Observation of L/H transition on Wendelstein VII-AS

We have analyzed data taken with a broadband X-mode heterodyne reflectometer [22] in the edge region of the Wendelstein VII-AS stellarator [23]. This is a low-shear modular stellarator with major radius $R_0 = 2$ m and minor radius $a \approx 0.18$ m. The toroidal magnetic field is $B = 2.5$ T. In the discharge investigated, the plasma was heated with $P_{ECH} = 400$ kW of ECRH power at 140 GHz. The central electron density was $n_e = 8 \times 10^{19}$ m^{-3}, while the central electron temperature was $T_e = 0.8$ keV. The rotational transform at the plasma edge was $\iota = 0.53$. We studied the L/H transition that is generally observed in this kind of discharges [24], i.e. a transition from a low (L) to high (H) energy confinement mode, which is always accompanied by a sudden reduction in the measured fluctuation levels of e.g. the electron density. Here we present the data from one discharge only which we deem sufficient for purposes of illustration of the data analysis technique, but refer to Ref. 25 for a more detailed study of the bicoherence in L/H transitions.

Data are taken at various radial positions, but in the following we focus on the radial position of about 15.5 cm, which is where the strongest reduction in the fluctuation level is observed during the L/H transition. This position is about 1 cm inside the separatrix. Fig. 8a shows the time development of the total bicoherence and of the RMS level of the reflectometry data, as well as the signal from the H_α-light emission detector. A sharp drop in the signal from the H_α detector is generally considered to be indicative of an L/H transition. The transition is seen to occur at 757.5 ms. The spikes in the H_α signal in the H-phase are caused by Edge Localized Modes (ELMs), whose nature is only partly understood. Observe that the L/H transition is clearly seen both on the total bicoherence and RMS signals. Note that before the transition (in the L-phase), the RMS value is high and the bicoherence is at noise level (dashed line). During the H-phase the bicoherence is clearly augmented (by a factor 2-3), whereas the RMS level has dropped by a similar factor. The apparent lack of correlation between the RMS level or the bicoherence and the occurrence of ELMS is entirely due to the low time resolution of these calculations; in reality, a clear correlation between the RMS level and the occurrence of ELMs exists. In the case of the bicoherence, the problem is more complicated, since the data corresponding to one ELM do not allow a calculation of the bicoherence with sufficient statistics to obtain reliable results; nevertheless, we investigated this question in a little more detail, results of which are presented below.

The interpretation of the measured phase of the reflectometer signal is complex, since the reflection does not occur in a single point, but in a nearly two-dimensional section of the plasma. Thus interference between signals received from various points may occur and obscure the local information [26, 27, 28]. When the scale lengths of turbulent structures are large enough (with respect to some antenna pattern that depends on the plasma density distribution), such effects may be deemed unimportant. But they become relevant when the structures are of the size of or smaller than the antenna pattern and the RMS of the fluctuations is high enough. Multiple-ray tracing simulations (which can account for the interference phenomena) indicate that under these two conditions an artificial increase in the bicoherence of the demodulated phase signal is observed (i.e. due to this interference rather than non-linear processes in the plasma). The observed low value of the bicoherence during the L mode suggests, however, that these two-dimensional effects are not very important here. The increase of the bicoherence at the L/H transition could therefore be due to a scale reduction of turbulent structures in the plasma. On the other hand, the observed reduction in the turbulence amplitudes (RMS) together with the increase of the density gradient during the H-mode implies that two-dimensional interference effects may be expected to be even weaker here than in the L-mode, which seems to favor an interpretation in terms of increased nonlinear interactions.

To gain some insight into the characteristics of the L- and H-phase and the ELMS, we calculated the bicoherence and the wavelet spectra on time sections of 1 ms length and summed the results. For the L-phase, 5 such sections were selected arbitrarily but before the transition at 757.5 ms. For the ELMs, these sections were chosen centered on the spikes in the RMS level,

corresponding to the 5 major spikes in the H_α signal (Fig. 8a); finally, for the H-phase, 5 sections were selected inbetween the ELMs. The summed wavelet bicoherence resulting from these calculations is presented in Fig. 8b; the bicoherence in Fig. 8c; and the wavelet spectra in Fig. 8d. In Fig. 8d it is seen that the wavelet power spectrum drops almost by an order of magnitude when going from L to H, in accordance with the drop in the RMS level seen earlier. The spectrum corresponding to the ELMs is inbetween, and a bit closer to the L-phase than the H-phase level. From the summed bicoherence graph in Fig. 8b it is clear that the bicoherence is close to noise level in the L phase, as expected from the earlier observation presented in Fig. 8a. The H-mode exhibits a high bicoherence at nearly all frequencies, with a peak at 50 kHz (Fig. 8b). There is a weak indication that this frequency couples to higher frequencies (Fig. 8c), but the graph is by no means conclusive. Finally, the ELMs exhibit a high bicoherence over a broad range of frequencies as well (Fig. 8b), and several broad peaks can be discerned (at 80 and 220 kHz), but the twodimensional graph (Fig. 8c) shows that the bicoherence here is quite different from the H-phase case, and it exhibits a complex structure.

Summarizing we believe that we can maintain, although we cannot make any statement about the nature of the ELMs, that an ELM is *not* simply a short return to L-mode conditions (which has been a working supposition for some time), but a rather more complex phenomenon involving nonlinear modes or phase coupling effects. This statement is based on the wavelet bicoherence analysis which shows that the phase coupling processes in the turbulence during ELMs are more similar to the situation in the H-phase than the L-phase, even though the RMS levels are more similar to the L-phase than the H-phase.

IV Conclusions

IV.a General conclusions concerning the analysis method

In this paper we have presented a new analysis method for turbulent data, based on wavelet analysis and bispectral analysis. The bispectrum is the first higher-order spectrum after the ordinary spectral analysis and is useful for the investigation of non-linear interactions of the lowest order (i.e. quadratic interactions). The novel technique presented here, wavelet bicoherence, detects phase coupling between short-lived wavelets rather than between modes (as with the Fourier bicoherence). Since modes with a long lifetime are not necessarily a part of turbulence this method is better adapted to the analysis of turbulent data. The use of wavelets imbues the analysis with time resolution, opening the possibility of (1) detecting intermittency of turbulence, and (2) detecting phase coupling in strong turbulence where the Fourier-based bicoherence averages out most of the relevant information (cf. Section II.c). Relatively short data sequences are sufficient to perform an analysis, in contrast to the Fourier bicoherence that needs long time series to obtain both sufficient frequency resolution and statistics. Estimates of

the noise contribution and error level of the wavelet bicoherence provide a criterion for the reliability of the results. A powerful noise reduction is an integral part of the standard technique: as non-coherent contributions are averaged out, weak coherent signals can be detected in very noisy data.

As a first application of the technique we mention the possibility of "fingerprinting" turbulence, i.e. the bicoherence graph for various types of turbulence is unlikely to be very similar, as indicated by the examples we have shown, and thus a classification based on the bicoherence graphs is perhaps possible.

Secondly, the bicoherence may provide a link between theoretical turbulence models and experimental measurements. Comparison of the bicoherence graphs yielded by the analysis of numerically generated and experimental data should provide an indication whether the turbulence models are suitable approximations of reality.

Finally, the numerical value of the bicoherence can in some cases be related to parameters of a given turbulence model (such as the coupling strength in the simple quadratic coupling model discussed in Section II.c). This may permit the quantification of the dynamics of the turbulence in those cases where an acceptable model is available.

An important question that may be posed is whether this technique is capable of detecting so-called 'coherent structures'. The difficulty in answering this question is partly caused by the lack of definition of this concept. However, if we adopt the working definition that a coherent structure is an object that shows spatial and temporal correlation in an otherwise uncorrelated background, then the answer is yes, provided it has some minimal size and lifetime, which are determined through the frequency and time resulution and the noise level as discussed in Section II. It should be noted, however, that with a single observation point it is not possible to distinguish between a static structure passing by the observation point and a dynamical quadratic wave-interaction process. Comparing this capability with the Biorthogonal Decomposition (BD) method [29, 30], we remark that the BD is capable of detecting coherent structures in the local frame of reference with relatively little interpretation problems; however, measuring in the local frame of reference is not always possible (and almost never in fusion experiments). The wavelet bicoherence, however, exhibits merely a Doppler shift when performing a Galileo transformation without losing the coupling information. Thus, the wavelet bicoherence is more independent of the frame of reference and may be expected to be more useful in experiments where measurement in the local frame of reference is difficult.

IV.b Summary of results

We have shown that the wavelet bicoherence provides information about turbulent signals that is not available from the usual data analysis methods. The bicoherence of turbulent data taken with Langmuir probes in a tokamak plasma (Section II.e) was seen to disappear when the signal was phase-randomized while maintaining the amplitude spectrum constant. Similarly, the

simulation of drift wave turbulence (Section III.b) showed a drop in the bicoherence at the mode rational surface that did not correspond to any distinct feature in the RMS value or the spectrum. We believe that these examples demonstrate that valuable information is contained in the bicoherence.

In order to examine further the meaning of the bicoherence, we have analyzed data from two model systems.

Firstly, the system consisting of two coupled van der Pol oscillators, considered to be one of the simplest systems that show self-sustained chaos without external driving, was analyzed (Section III.a). The system parameters were selected to produce both a quasiperiodic and a chaotic state. It was found that in the quasiperiodic state the bicoherence provided accurate information about the coupling interaction between the two oscillators. In the (weakly) chaotic state the coupling interaction could still be identified in the twodimensional bicoherence graph, along with the effects of the period-doubling transition to chaos.

Secondly, a plasma drift wave model in sheared slab geometry was analyzed (Section III.b). This model bears relevance to the turbulence occurring in thermonuclear fusion plasmas. The presence of a coherent structure was deduced accurately from the total bicoherence vs. radial position graph to be located near (but not *at*) the $q = \frac{3}{2}$ rational surface. This coherent structure was subsequently seen in the twodimensional graphs of ion density vs. poloidal and radial position. Further, a drop in bicoherence at the mode rational surface indicated a possible destruction of coherent structures by enhanced shear flow at that position. Finally, the coupling of the resonant mode to broad-spectrum turbulence was observed.

Experimental data taken with reflectometers in thermonuclear fusion plasma experiments were also analyzed.

Firstly, a clear indication of intermittency was found in the case of ATF (Section III.c). Similar observations were reported earlier for the same device [1]. It was found that the intermittent part of the bicoherence is mainly due to high frequencies (> 100 kHz).

Secondly, data from Wendelstein VII-AS taken during the L/H transition (Section III.d) showed a notable increase in the total bicoherence level at the transition. No clear correlation of the bicoherence level and the occurrence of ELMS during the H-mode was found, even though there exists a strong correlation between the RMS value of the signal and the occurrence of an ELM. The bicoherence graph obtained by summing the data from 5 ELMS was seen to have the same overall level of bicoherence as the data obtained from 5 data sections from the H mode, but to have a more complex structure.

IV.c Future developments

The technique for wavelet bicoherence as presented in this paper is based on the simple wavelet as given by Eq. (14). This wavelet has the advantage that it removes the unrealistic assumption that the turbulent signals that are analyzed consist of modes that are constant in time, while it

preserves to some degree the physical intuition associated with the mode paradigm (i.e. by assigning a frequency to each wavelet scale one may continue to speak in terms of coupling between frequencies). The latter feature greatly facilitates the interpretation of the bicoherence, but it may not allways be adequate. In particular, while this wavelet may be appropriate for weakly developed turbulence, perhaps the point of view that the signal is constituted of regular (if short-lasting) oscillations is no longer valid in fully developed turbulence. One may therefore consider substituting the analyzing wavelet by more appropriate ones, such as the "Mexican Hat" wavelet mentioned in literature [7]. In that case, however, the language referring to frequencies should be abandoned altogether and one should refrain to speaking in terms of scales.

A further step in the analysis of turbulence based on bicoherence analysis would be the calculation of energy transfer between frequencies. The principles of this technique are established in e.g. Ref. 10. As mentioned before, however, such calculations require the adoption of a turbulence model (e.g. the quadratic coupling model), the validity of which is open to discussion.

It has been suggested to proceed to the calculation of even higher-order spectra than the third-order bispectrum. The difficulty here is not mathematical, since the generalization of the bispectrum to higher orders is straightforward, but practical: the representation of such high-order spectra is the limiting factor. Perhaps new powerful computer visualizing tools may open up this direction of development in the near future.

Finally, while in this paper we have concentrated on the analysis of time series data, we believe that in the analysis of turbulence it is important to include spatial information in the analysis. In fusion plasmas, it is a difficult problem by itself to obtain time- *and* space-resolved data; nevertheless some are available (e.g. Ref. 31) and more are expected. It is not clear *a priori* how bicoherence analysis could be generalized to such data.

Acknowledgements

This work was made possible by Commission of the European Communities Bursary ERB4001GT921485. The authors are endebted to I. Pastor and A. Lopez Fraguas for their kindness in sharing their data of and knowledge about van der Pol oscillators with us and for stimulating discussions. Likewise, they express their gratitude to their colleages at ATF and at Wendelstein who have generously shared their data with us. Finally, they would like to thank their other colleagues at the Asociación EURATOM-CIEMAT for a very pleasant cooperation.

References

[1] B. Ph. van Milligen, C. Hidalgo and E. Sánchez, Phys. Rev. Lett. **74**, 3 (1995) 395

[2] H.D.I. Abarbanel, R. Brown, J.J. Sidorovich, L. Sh. Tsimring, Rev. Mod. Phys. **65**, 4 (1993) 1331

[3] A.M. van den Brink, G.J.J. Remkes, F.C. Schüller and A.C.C. Sips, in Contr. Fusion and Plasma Phys. (Proc. 17th Eur. Conf. Amsterdam, 1990), Vol. 14B, Part I, European Physical Society (1990) I-199

[4] E. Ott, *Chaos in dynamical systems*, Cambridge University Press (1993) 266 - 291

[5] M. Farge, *The continuous wavelet transform of two-dimensional fluid flows*, in Wavelets and their applications, Ed. M.B. Ruskai et al., Jones and Bartlett Publishers, Boston, MA 02116 (1992) 275

[6] L. Hudgins, C.A. Friehe, M.E. Mayer, Phys. Rev. Lett. **71**, 20 (1993) 3279

[7] C. Meneveau, J. Fluid Mech. **232** (1991) 469

[8] Y.C. Kim and E.J. Powers, Phys. Fluids **21** (8) (1978) 1452

[9] Y.C. Kim, J.M. Beall and E.J. Powers, Phys. Fluids **23** (2) (1980) 258

[10] Ch. P. Ritz, E.J. Powers and R.D. Bengtson, Phys. Fluids **B 1** (1) (1989) 153

[11] Ch. P. Ritz, E.J. Powers, T.L. Rhodes, R.D. Bengtson, K.W. Gentle, Hong Lin, P.E. Phillips, A. J. Wootton, D.L. Brower, N.C. Luhmann, Jr., W.A. Peebles, P.M. Schoch and R.L. Hickok, Rev. Sci. Instrum. **59** (8) (1988) 1739

[12] I. Daubechies, *Ten Lectures on Wavelets*, National Science Foundation Series In Applied Mathematics, S.I.A.M. (1992)

[13] C. Chui, *An introduction to wavelets*, Academic Press, New York (1992)

[14] D.E. Newland, *An introduction to random vibrations, spectral & wavelet analysis*, Longman Scientific & Technical, New York, 3rd edition, ISBN 0582 21584 6 (1993) 295

[15] C. Hidalgo, E. Sánchez, T. Estrada, B. Brañas, Ch. P. Ritz, T. Uckan, J. Harris and A.J. Wootton, Phys. Rev. Lett. **71**, 19 (1993) 3127

[16] N. Mattor and P.W. Terry, Phys. Fluids. B **4** (5) (1992) 1126

[17] J.F. Lyon, B.A. Carreras, K.K. Chipley, M.J. Cole, J.H. Harris, T.C. Jernigan, R.L. Johnson, V.E. Lynch, B.E. Nelson, J.A. Rome, J. Sheffield and P.B. Thompson, Fusion Technol. **10** (1986) 179

[18] C. Hidalgo, B. Brañas, T. Uckan, J.H. Harris, R. Isler, Ch. P. Ritz and A. Wootton, Phys. Plasmas **1** (1994) 3

[19] I. Pastor, V.M. Pérez-García, F. Encinas-Sanz and J.M. Guerra, Phys. Rev. E, **48**, 1 (1993) 171

[20] B.A. Carreras, K. Sidikman, P.H. Diamond, P.W. Terry and L. Garcia, Phys. Fluids B **4** (10) (1992) 3115

[21] G.R. Hanson, J.B. Wilgen, E. Anabitarte, J.D. Bell, J.H. Harris, J.L. Dunlap and C.E. Thomas, Rev. Sci. Instrum. **61** (1990) 3049

[22] H.J. Hartfuß, T. Estrada, M. Hirsch, T. Geist and J. Sanchez, Rev. Sci. Instrum. **65** (7) (1994) 2284

[23] H. Renner, WVII-AS Team, NBI Group, ICF Group, and ECRH Group, Plasma Phys. Controlled Fusion **31** (1989) 1579

[24] V. Erckmann, F. Wagner, J. Baldzuhn, R. Brakel, R. Burhenn, U. Gasparino, P. Grigull, H. J. Hartfuss, J. V. Hofmann, R. Jaenicke, H. Niedermeyer, W. Ohlendorf, A. Rudyj, A. Weller, S. D. Bogdanov, B. Bomba, A. A. Borschegovsky, G. Cattanei, A. Dodhy, D. Dorst, A. Elsner, M. Endler, T. Geist, L. Giannone, H. Hacker, 0. Heinrich, G. Herre, D. Hildebrandt, V. I. Hiznyak, V. I. Il'in, W. Kasparek, F. Karger, M. Kick, S. Kubo, A. N. Kuftin, V. I. Kurbatov, A. Lazaros, S. A. Malygin, V. I. Malygin, K. McCormick, G. A. Müller, V. B. Orlov, P. Pech, H. Ringler, I. N. Roi, F. Sardei, S. Sattler, F. Schneider, U. Schneider, P. G. Schüller, G. Siller, U. Stroth, M. Tutter, E. Unger, H. Wolff, E. Würsching and S. Zöpfel, Phys. Rev. Lett. **70** (1993) 2086

[25] T. Estrada, M. Hirsch, T. Geist, H.J. Hartfuss, J. Sánchez, E. Sánchez, C. Hidalgo, B. Ph. van Milligen, E. de la Luna, in Contr. Fusion and Plasma Phys. (Proc. 21th Eur. Conf. Montpellier, 1994), Vol. 18B, Part I, European Physical Society (1994) I-404

[26] J. H. Irby, S. Horne, I.H. Hutchinson and P.C. Stek, Plasma Phys. Control. Fusion **35** (1993) 601

[27] E. Mazzucato and R. Nazikian, Plasma Phys. Control. Fusion **33** (1991) 261

[28] E. Mazzucato and R. Nazikian, Phys. Rev. Lett. **71** (1993) 1840

[29] N. Aubry, M.-P. Chauve and R. Guyonnet, Phys. Fluids **6**, 8 (1994) 2800

[30] Th. Dudok de Wit, Enhancement of Multichannel Data in Plasma Physics by Biorthogonal Decomposition, Submitted to Plasma Physics and Controlled Fusion (1994)

[31] S.J. Zweben and R.W. Gould, Nucl. Fusion, **35**, 2 (1985) 171

Table 1: System parameters for the coupled van der Pol oscillators in a periodic and a chaotic state

System state	ε_1	ε_2	α_1	α_2
Periodic	1.0	1.0	0.5	-1.75
Chaotic	1.0	1.0	0.5	1.75

Figures

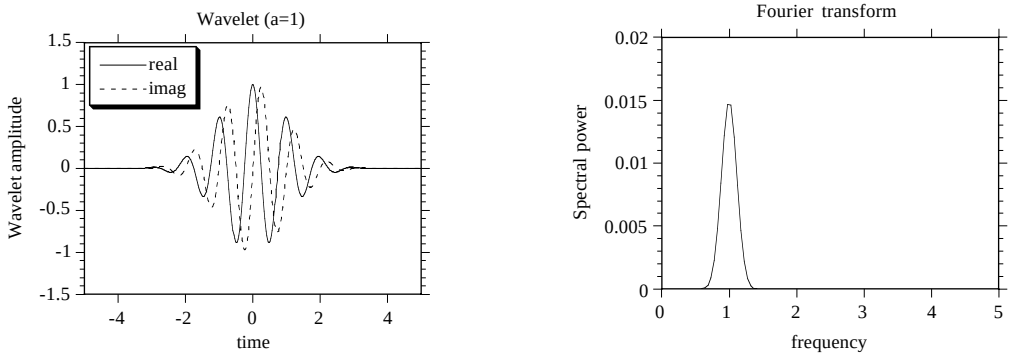

Fig. 1 Analyzing wavelet amplitude and Fourier transform. Similar plots for wavelets at other scales can be obtained by means of the scaling transformations:

$$\Psi_a(t) = \frac{1}{\sqrt{a}}\Psi(t/a) \quad and \quad \hat{\Psi}_a(\omega) = \sqrt{a}\,\hat{\Psi}(\omega a)$$

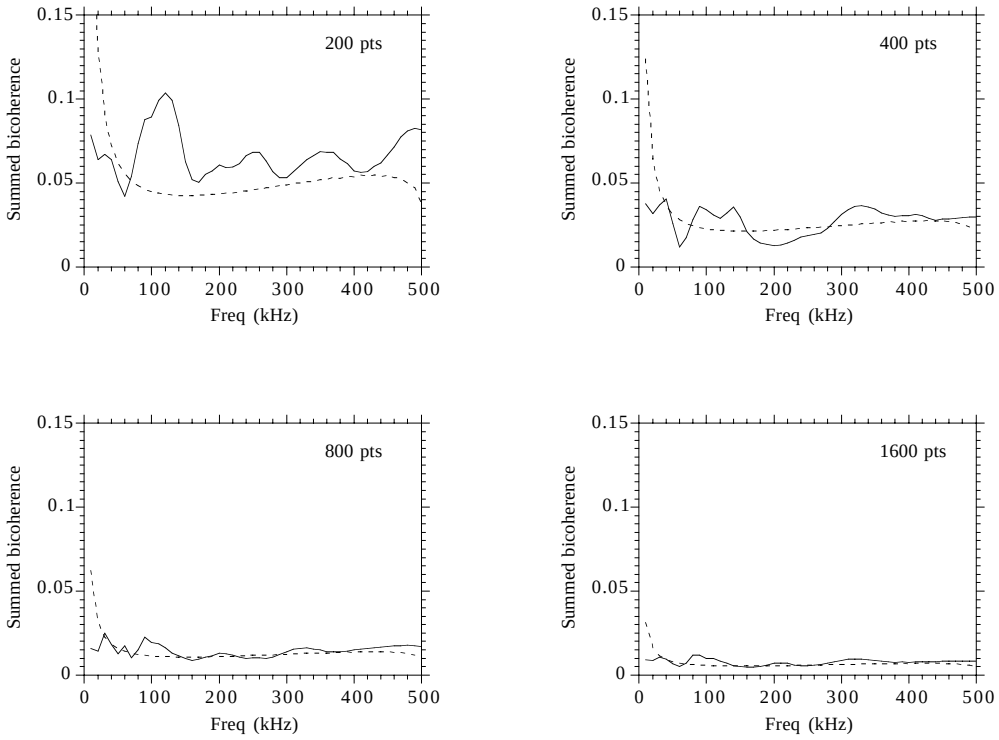

Fig. 2 Summed wavelet bicoherence of a random time series with a Gaussian PDF sampled at 1 MHz. The analysis is performed on sections with N = 200, 400, 800 and 1600 data points. The bicoherence (solid line) falls roughly as predicted by the theoretical noise level estimate, Eq. (16) (dashed line).

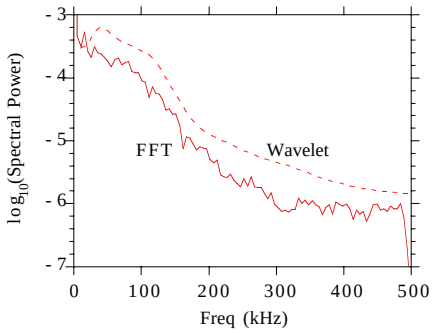

Fig. 3a Spectral analysis of data (from 1 to 9.192 ms) taken with Langmuir probes at ATF; shown is the base-10 logarithm of the spectral power for both the smoothed Fourier spectrum and the wavelet spectrum (with arbitrary offset).

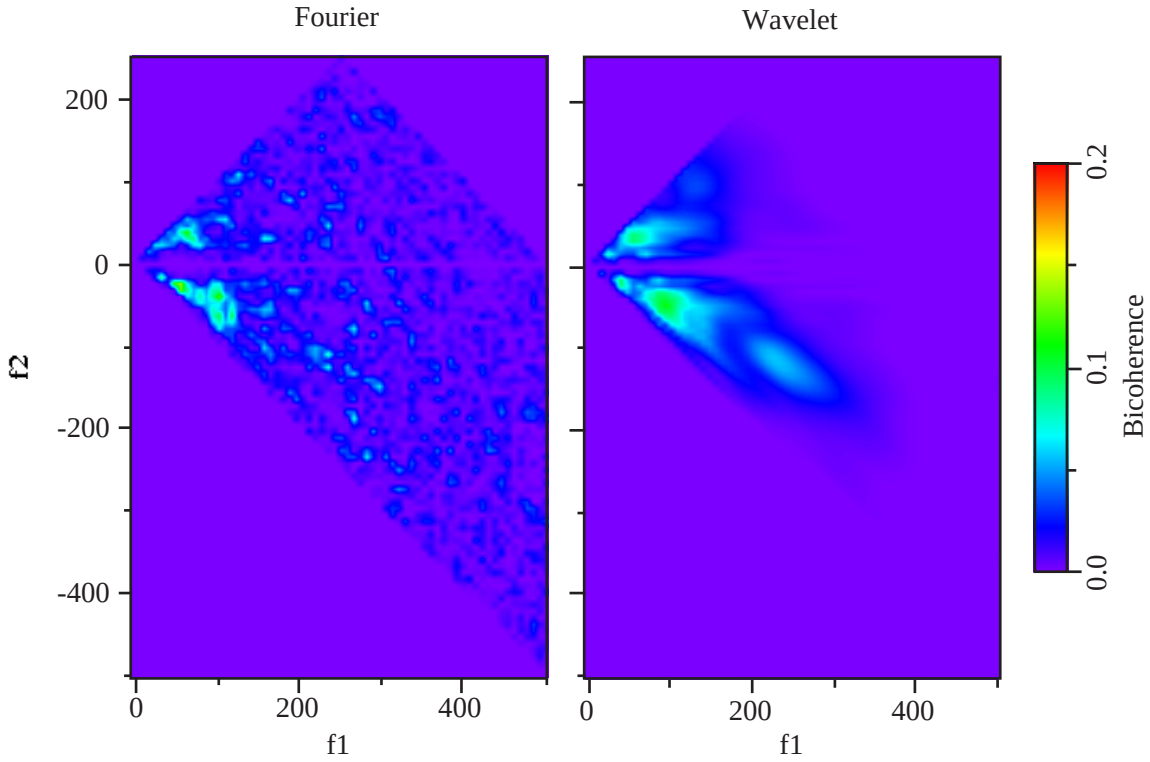

Fig. 3b Fourier and wavelet bicoherence graphs, calculated on a frequency grid with 64 grid points from 0 to 500 kHz on a data section from 1 to 16 ms.

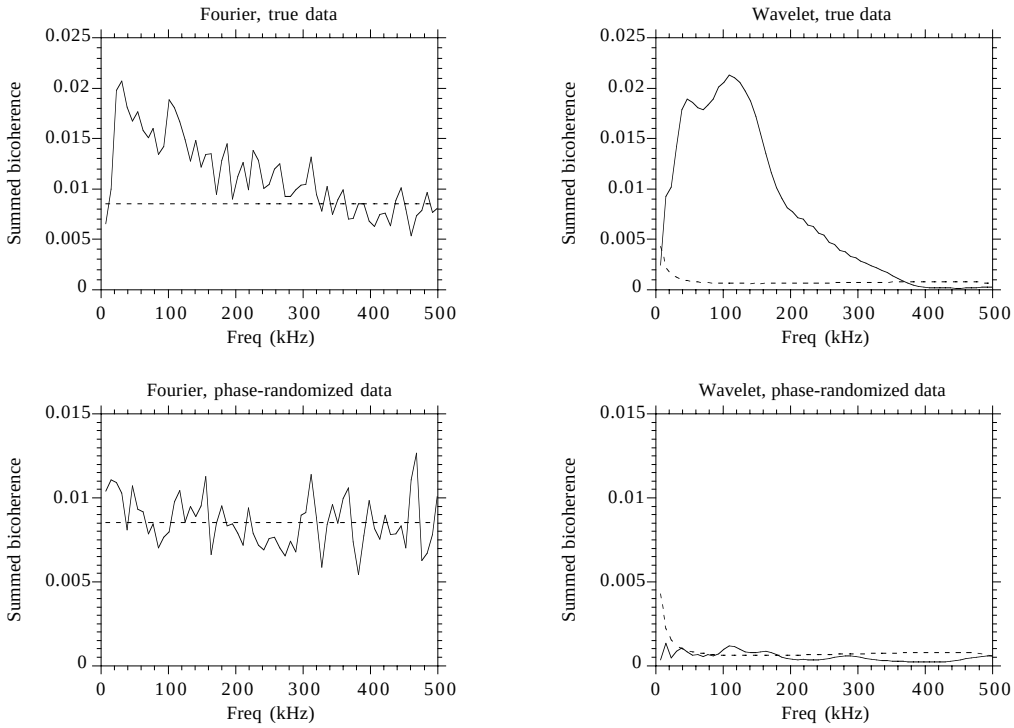

Fig. 3c (top) The summed bicoherence for both the Fourier and Wavelet bicoherence. (bottom) The summed bicoherence for both the Fourier and Wavelet bicoherence after scrambling the phase information in the data (see text). As expected, the bicoherence drops to noise level.

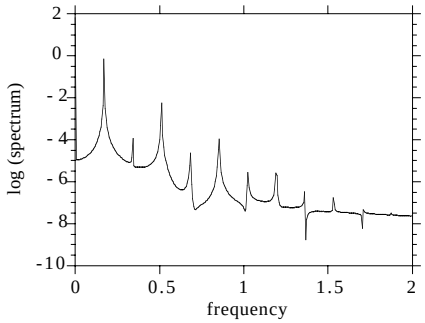

Fig. 4a Coupled van der Pol oscillators, periodic state, Fourier spectrum

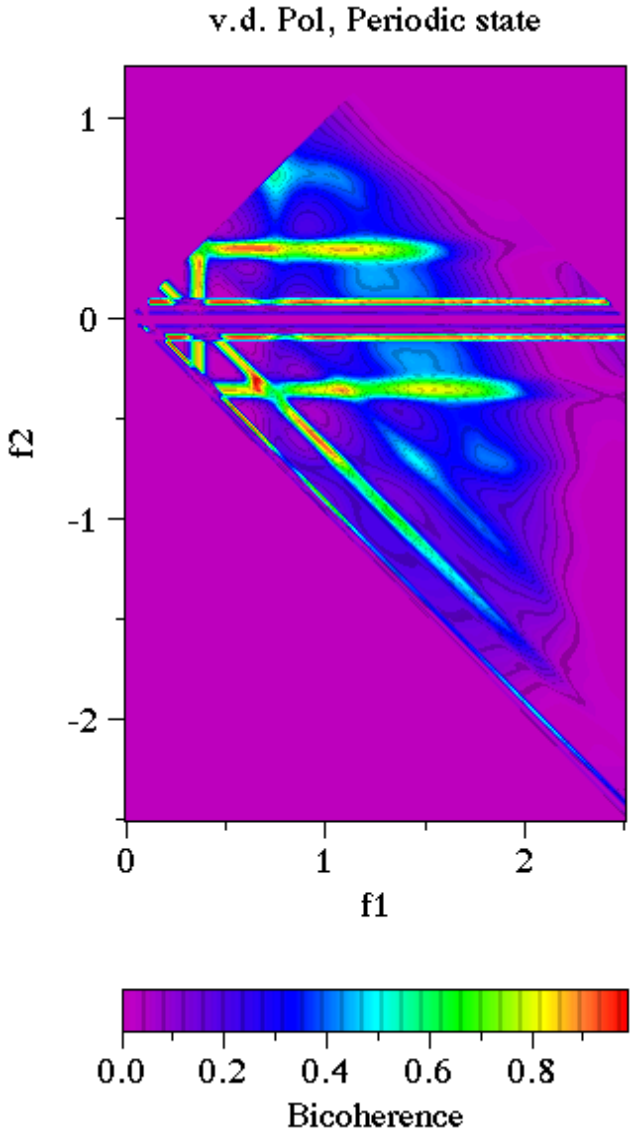

Fig. 4b Coupled van der Pol oscillators, periodic state, bicoherence taken over 153 data points covering about 5 periods of the x_2 coordinate. The very clear horizontal and diagonal ridges are due to the coupling between the two oscillators at a frequency of 0.34.

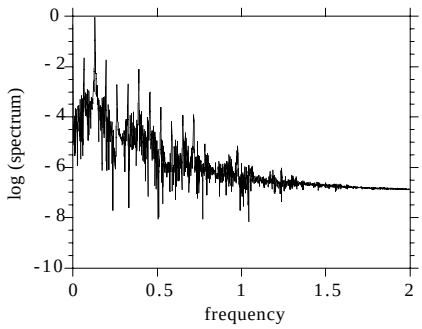

Fig. 4c Coupled van der Pol oscillators, chaotic state, Fourier spectrum

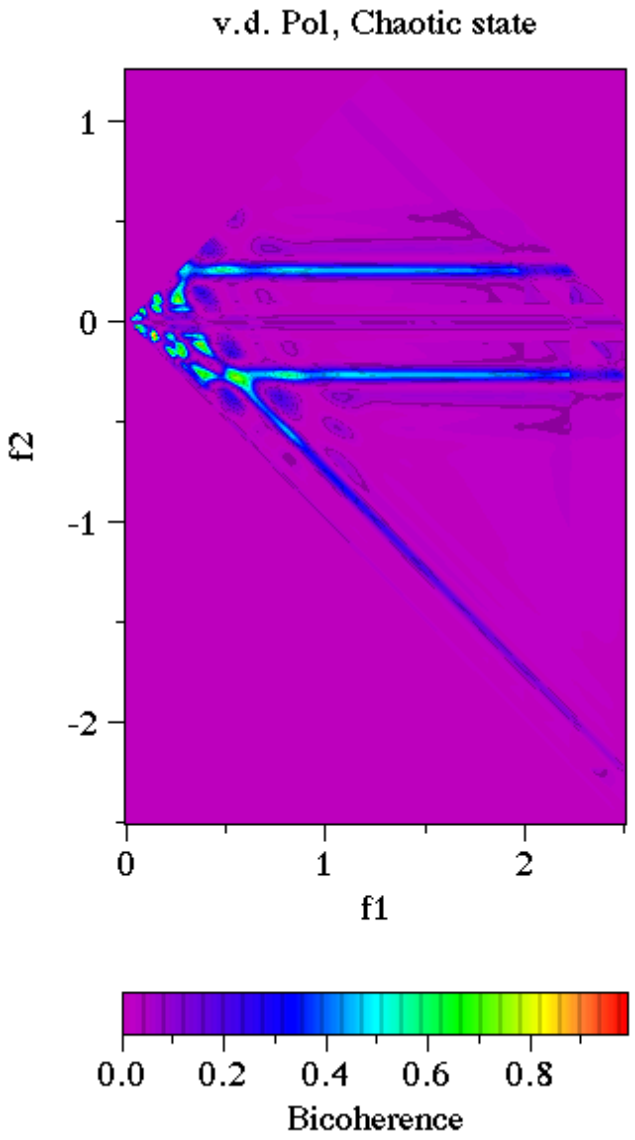

Fig. 4d Coupled van der Pol oscillators, chaotic state, bicoherence taken over 303 data points covering about 8 pseudo-periods of the x_2 coordinate. The overall structure is reminiscent of Fig. 4a (although the change in control parameters induced a frequency downshift of the main coupling frequency to 0.25), but the transition to chaos by means of period doubling has introduced a more complex structure at low frequencies.

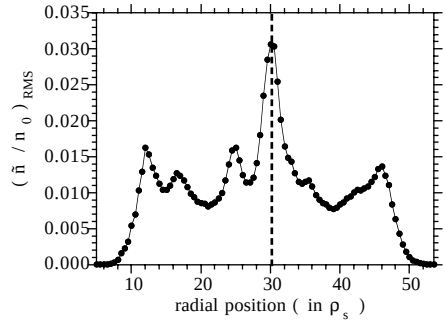

Fig. 5a RMS fluctuation level vs. radius of the ion density in the sheared slab drift wave model discussed in the text.

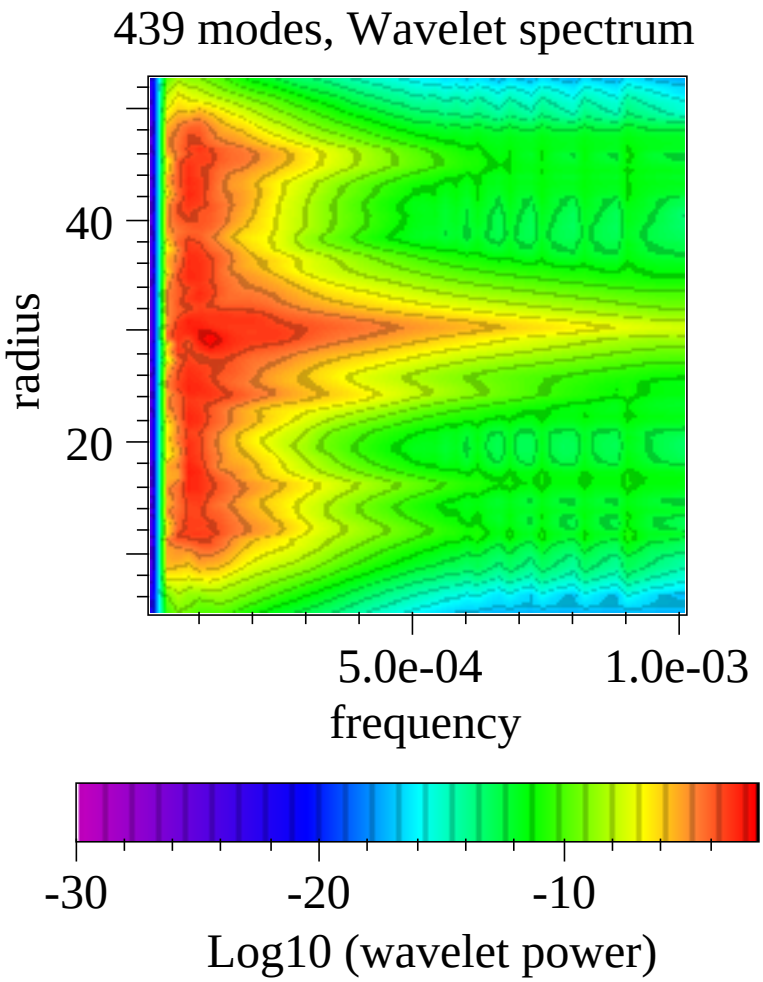

Fig. 5b Wavelet spectrum vs. radius for the same data as in Fig. 5a.

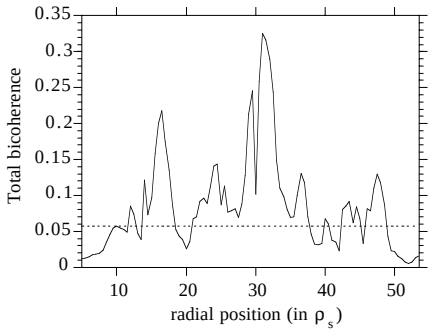

Fig. 6a Total wavelet bicoherence vs. radial position for the same data as in Fig. 5.

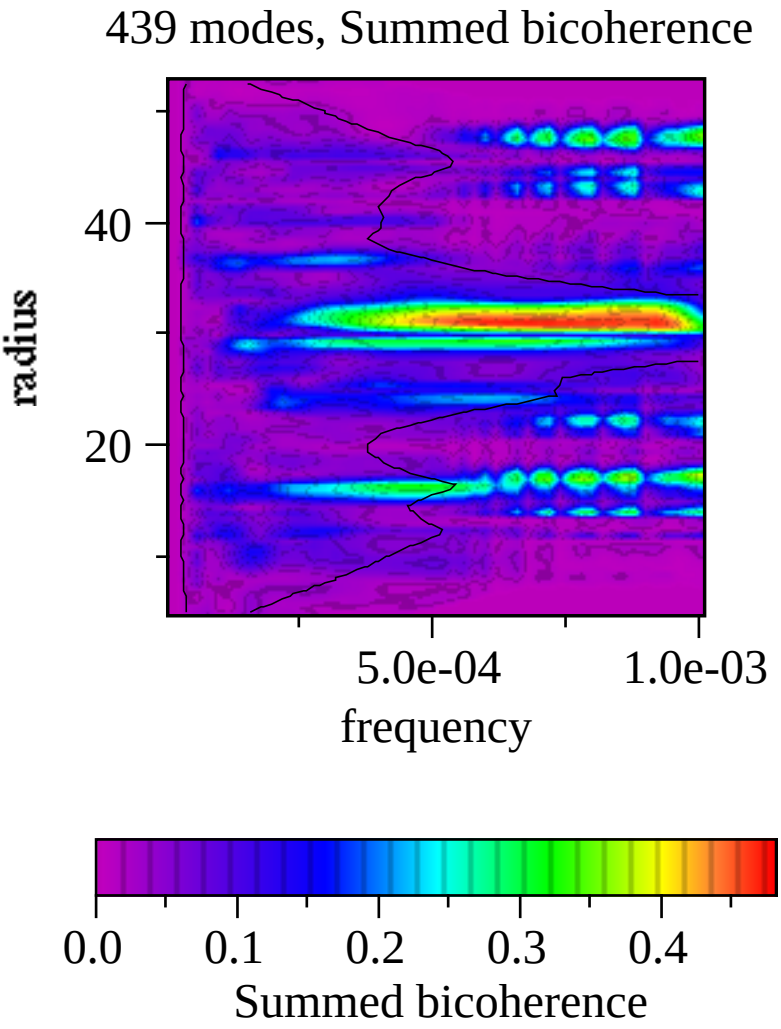

Fig. 6b Summed wavelet bicoherence vs. radial position and sum frequency. The dashed line (a contour taken from Fig. 5b at log(wavelet power) = -10) indicates roughly up to what frequency the bicoherence may be considered reliable.

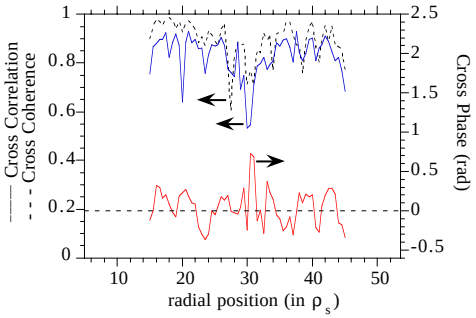

Fig. 6c Cross correlation, cross coherence, and cross phase between adjacent channels. Results are shown at position x ρ_s for the cross analysis between x ρ_s and (x+0.5) ρ_s. The cross coherence and -phase are computed from FFT (cross) spectra and are averaged over all frequencies by weighing with the spectral power.

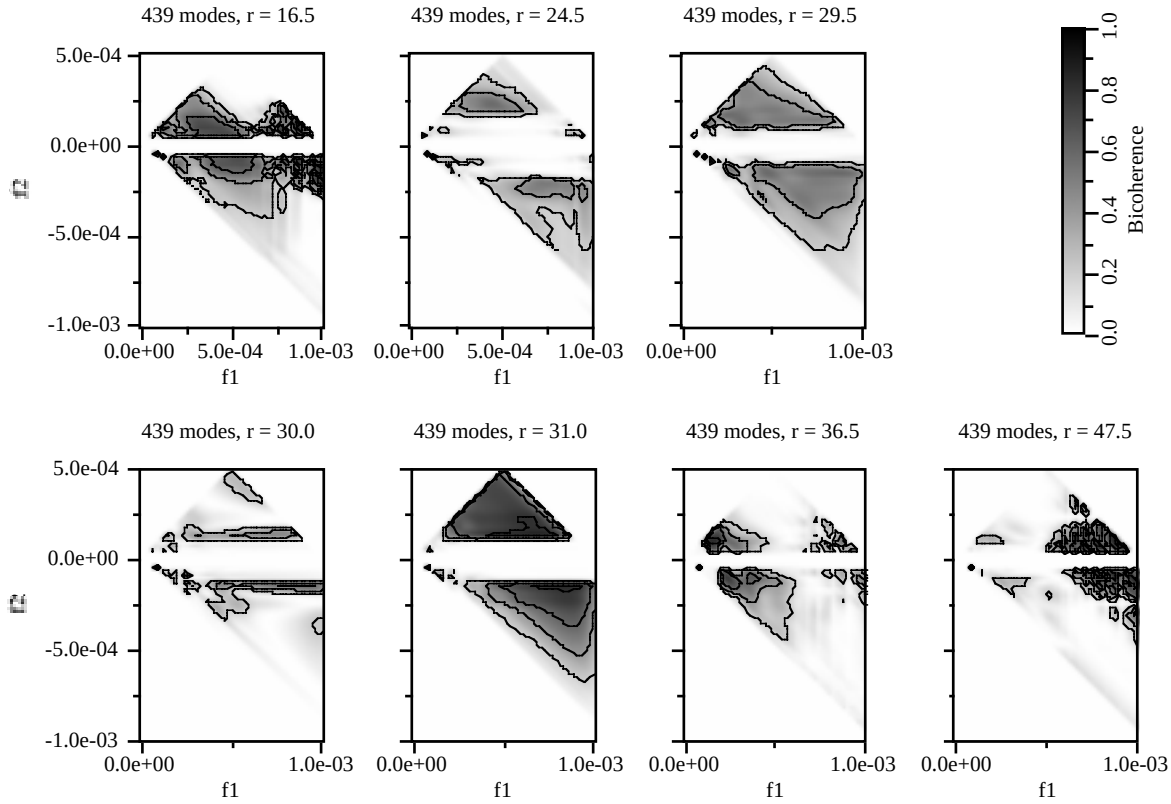

Fig. 6d Bicoherence for some selected radii.

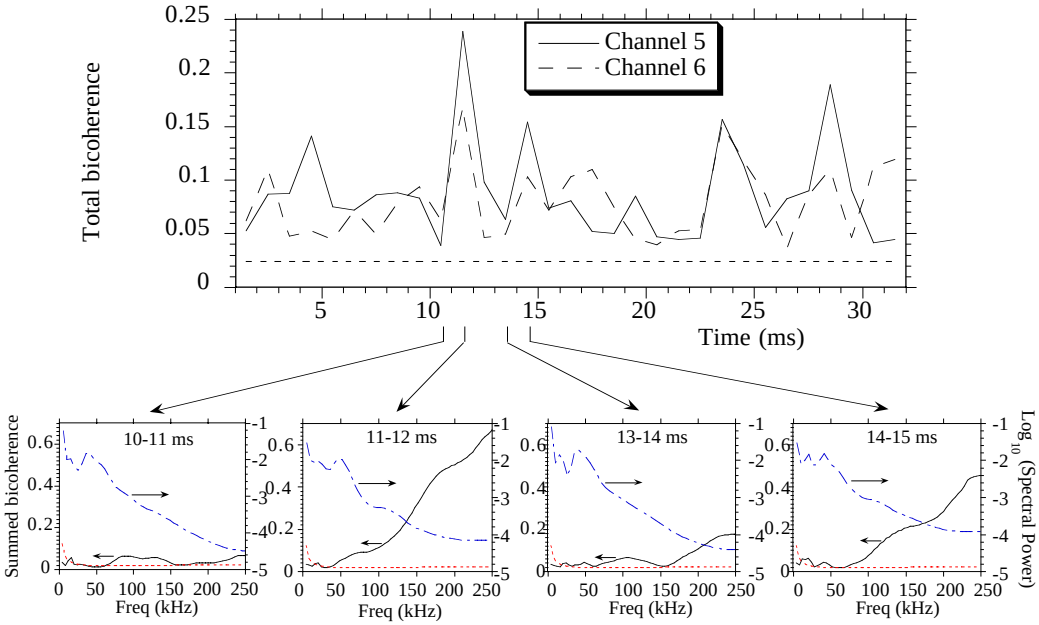

Fig. 7a ATF Reflectometry, summed bicoherence vs. time, shot 11271.5. This shot exhibits both very strong Fourier and wavelet bicoherence. The strong variation with time is an indication of turbulent intermittency. The summed bicoherence graphs at various times show that the temporally intermittent part of the coupling is mainly due to high frequencies (above 100 kHz). For reference, the corresponding wavelet spectra are also shown.

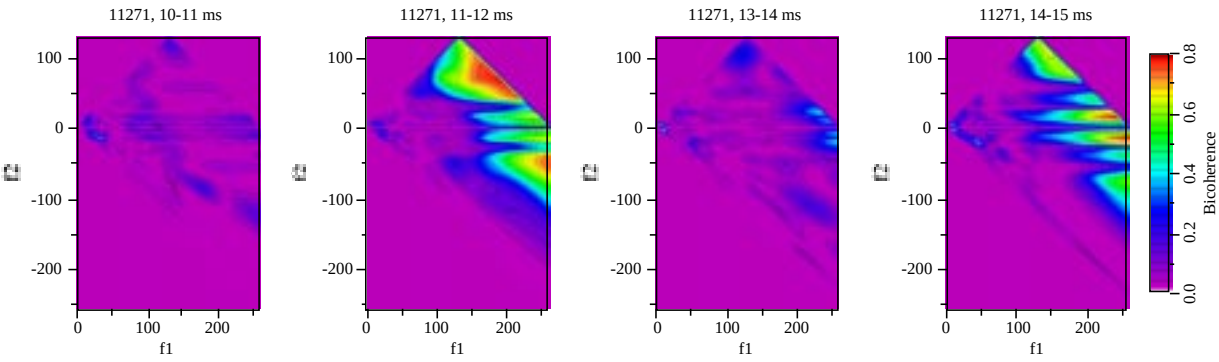

Fig. 7b Series of bicoherence plots corresponding to the time intervals of Fig. 10a. Note the similarity of the graphs corresponding to high bicoherence (11-12 ms and 14-15 ms) to the simulations done by Carreras of drift-wave turbulence (Fig. 6).

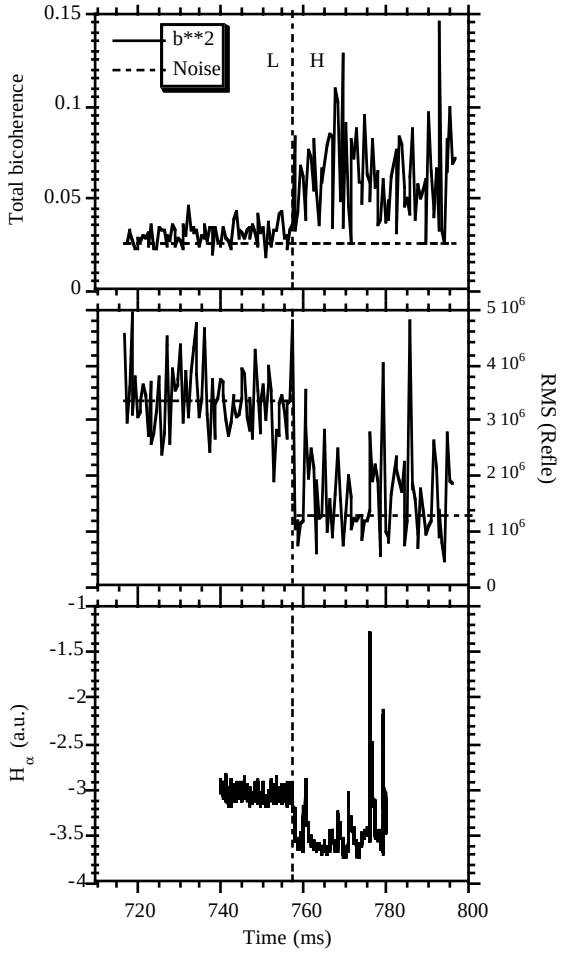

Fig. 8a Plots of the total bicoherence and RMS of the raw reflectometry signal taken at Wendelstein VII-AS, and the fast Hα signal. The L/H transition is marked by a vertical dashed line and shows up clearly in all graphs.

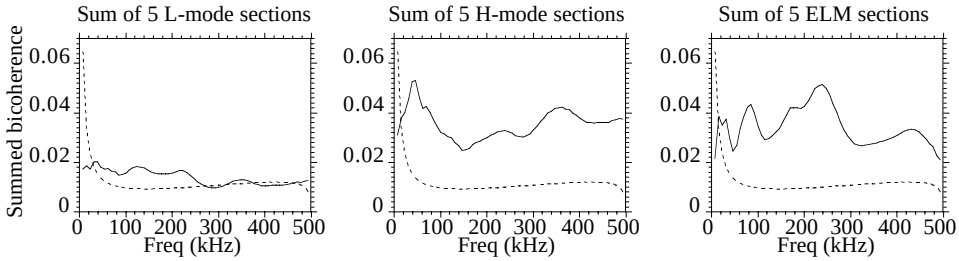

Fig. 8b Summed bicoherence graphs obtained by averaging the bicoherence data from several time windows of 1 ms each: 5 L-mode sections (742-743 ms; 744-745 ms; 746-747 ms; 748-749 ms; 750-751 ms); 5 H-mode sections (758-759 ms; 761-762 ms; 762.2-763.2 ms; 763.4-764.4 ms; 779.6-780.6 ms) and 5 sections containing ELMS (760-761 ms; 767.7-768.7 ms; 770.2-771.2 ms; 775.9-776.9 ms; 778.6-789.6 ms).

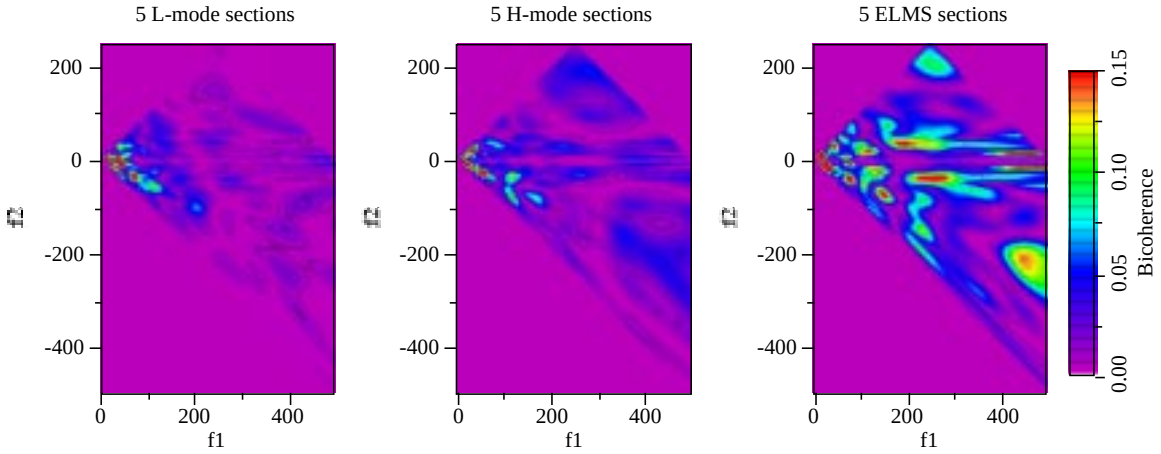

Fig. 8c Bicoherence graphs corresponding to Fig. 8b.

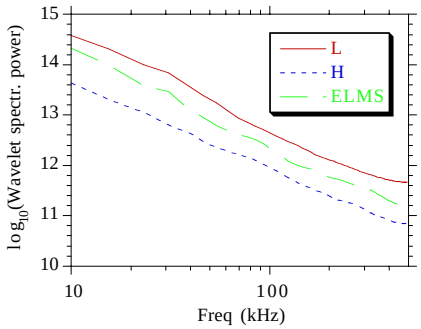

Fig. 8d Wavelet spectra, averaged over the time windows as given in the caption of Fig. 8b.